Cumulative analysis of the association between the data of the gravitational wave detectors NAUTILUS and EXPLORER and the gamma ray bursts detected by BATSE and BeppoSAX

P. Astone,[1] D. Babusci,[2] M. Bassan,[3,4] P. Carelli,[5,4] E. Coccia,[3,4,6] C. Cosmelli,[7,1] S. D'Antonio,[4] V. Fafone,[2] F. Frontera,[8,9] G. Giordano,[2] C. Guidorzi,[8] A. Marini,[2] Y. Minenkov,[3,4] I. Modena,[3,4] G. Modestino,[2] A. Moleti,[3,4] E. Montanari,[8,10] G. V. Pallottino,[7,1] G. Pizzella,[3,2] L. Quintieri,[2] A. Rocchi,[3,2] F. Ronga,[2] L. Sperandio,[2] R. Terenzi,[11,4] G. Torrioli,[7] and M. Visco[11,4]

[1]*INFN, Sezione di Roma, P.le Aldo Moro 2, I-00185, Roma, Italy*
[2]*INFN, Laboratori Nazionali di Frascati, via Enrico Fermi 40, I-00044, Frascati (Roma), Italy*
[3]*Dipartimento di Fisica dell'Università "Tor Vergata", via della Ricerca Scientifica 1, I-00133, Roma, Italy*
[4]*INFN, Sezione di Roma II, via della Ricerca Scientifica 1, I-00133, Roma, Italy*
[5]*Dipartimento di Fisica dell'Università, via Vetoio (Coppito 1), I-67010, Coppito (L'Aquila), Italy*
[6]*INFN, Laboratori Nazionali del Gran Sasso, S.S. 17 bis km 18.910, I-67010, Assergi (L'Aquila), Italy*
[7]*Dipartimento di Fisica dell'Università "La Sapienza", P.le Aldo Moro 2, I-00185, Roma, Italy*
[8]*Dipartimento di Fisica dell'Università, via Paradiso 12, I-44100, Ferrara, Italy*
[9]*CNR, Istituto di Astrofisica Spaziale e Fisica Cosmica, via Piero Gobetti 101, I-40129, Bologna, Italy*
[10]*ISA "A.Venturi", Modena, Italy*
[11]*CNR, Istituto di Fisica dello Spazio Interplanetario, via del Fosso del Cavaliere 100, I-00133, Roma, Italy*

(Received 11 November 2004; published 14 February 2005)

The statistical association between the output of the Gravitational Wave (GW) detectors EXPLORER and NAUTILUS and a list of Gamma Ray Bursts (GRBs) detected by the satellite experiments BATSE and BeppoSAX has been analyzed using cumulative algorithms. GW detector data collected between 1991 and 1999 have been searched for an energy excess in a 10 s interval around the GRB flux peak times. The cumulative analysis of the data relative to a large number of GRBs (387) allows to push the upper bound for the corresponding GW burst amplitude down to $h = 2.5 \times 10^{-19}$.

DOI: 10.1103/PhysRevD.71.042001 PACS numbers: 04.80.Nn, 07.05.Kf, 98.70.Rz

I. INTRODUCTION

Since 1991, almost 3000 Gamma Ray Bursts (GRBs) have been detected by the satellite experiments BATSE [1,2] and BeppoSAX [3,4]. The large database [5–7] now available includes information about the GRB arrival time, duration, intensity in some frequency bands, sky position of the source, and (for a small GRB subset) redshift. The observation of a large number of GRBs, which are likely associated to catastrophic events capable of producing large GW signals, has given the possibility of systematic analysis of the GW detector data around the GRB arrival times. This is very important, because GW data analysis in association with GRBs can profit of a number of useful information (GRB time, source position, intensity *etc.*) and both positive and negative results could be given a direct astrophysical interpretation. Cumulative data analysis techniques have been developed to detect a statistically significant association between GW signals and GRBs [8–12]. Using for the first time a cross-correlation method applied to the data of two GW detectors, EXPLORER and NAUTILUS, experimental upper limits were determined for the amplitude of the GW bursts associated with GRBs [13]. Analyzing the data for 47 GRBs detected by BeppoSAX, the presence of GW pulses of amplitude $h \geq 1.2 \times 10^{-18}$ was excluded with 95% probability, within the time window of $\pm$ 400 s. Within the time window of ± 5 s, the upper limit was improved to $h = 6.5 \times 10^{-19}$.

Searching for an association between the two emissions, the main difficulty arises from the theoretical uncertainty in the delay between the GRB and GW arrival times. All the theoretical models presently available [14–20], and the interpretation of experimental observations of GRB characteristics [21–23], foresee that the GRB generation can happen during different phases of catastrophic events involving binary systems or massive stars. During some of these phases, the GW emission could happen at the same time as the GRB one. Thus, it is interesting to apply cumulative techniques making the restrictive hypothesis of simultaneity of the GRB and GW emissions. Implicitly making this hypothesis, several analyses have been performed [24–26]. In [26] an upper limit of $h = 1.5 \times 10^{-18}$ on the average amplitude of GW associated to GRBs was obtained with the resonant bar detector AURIGA, using 120 GRBs and an integration time window of 10 s.

According to the present knowledge of the GRB physics, at distance of 1 Gpc, GW burst signals of the order of $h \sim 10^{-22}$ or smaller are expected in association with GRBs. At the time the data used here were taken, EXPLORER and NAUTILUS were probably the most sensitive GW detectors, having a sensitivity for one ms duration GW burst with signal-to-noise ratio equal to unity of about 10^{-18} in h, further improved in the following years [27]. Thus we expect a null result, which, however, can be used to set upper limits to the GW flux. The present limits need to be significantly improved to get useful constraints on current

GRB theoretical models. Recently, the large interferometric GW detectors are beginning to come into operation, and in particular LIGO is reaching a sensitivity that allows to start looking at correlation with GRBs [28].

In Sec. II the data and the cumulative algorithms used in this work will be described [29]. The results will be shown and discussed in Sec. III.

II. DATA AND METHOD

The ROG Collaboration operates two resonant bar detectors: EXPLORER since 1990 at the CERN laboratory and NAUTILUS since 1995 at the INFN laboratory in Frascati. The two detectors, oriented nearly parallel, are very similar. They consist of massive cylindrical bars 3 m long made of high quality factor aluminum alloy 5056. The GW excites the first longitudinal mode of the bar which is cooled to liquid helium temperature to reduce the thermal noise. To measure the bar strain induced by a GW, a secondary mechanical oscillator tuned to the antenna mode is mounted on one bar face (as a consequence we have two resonant modes) and a sensor measures the displacement between the secondary oscillator and the bar face. The frequencies of these resonant modes varied slightly during the years, remaining for both antennas in the range 900–940 Hz. The data considered in the present analysis are sampled with a sampling time of 0.2908 s and processed with an adaptive Wiener filter [30]. The Wiener filtered data represent the energy innovation (expressed in kelvin) of each of the two modes. For each data sample, the minimum energy between the two modes is taken, obtaining the ''minimum'' mode time series, $E(t)$, which is the one used in this analysis. The probability distribution of $E(t)$ is

$$f(E) \propto \frac{1}{T_{\rm eff}} e^{-E/T_{\rm eff}}, \tag{2.1}$$

where $T_{\rm eff}$, called *effective temperature* and expressed in kelvin units, gives an estimate of the noise. In our analysis data stretches of 30 min duration were considered, centered at the arrival times of the GRBs. In Fig. 1, the distribution of $T_{\rm eff}$ is shown for 1150 data stretches selected for the analysis. The upper histogram corresponds to the EXPLORER data, the second one to the NAUTILUS data.

As regards the quality of the GW data, in order to improve the sensitivity of the analysis, we only consider the data stretches with effective temperature lower than 15 mK. In addition, we request that the ratio between the standard deviation and the average of each GW data stretch (this ratio is expected to be unity for an exponential distribution) lies between 0.8 and 1.5. These selection criteria restrict the data set to 387 GRBs. As GRB arrival time, we define the time of the flux peak on the 1024 ms trigger time scale extracted from the *Flux and Fluence Table* of *BATSE Current GRB Catalog* [7], while for BeppoSAX the GRB peak time is given by the time of the peak flux on a 1 s integration time. The GRB data also provide the angular

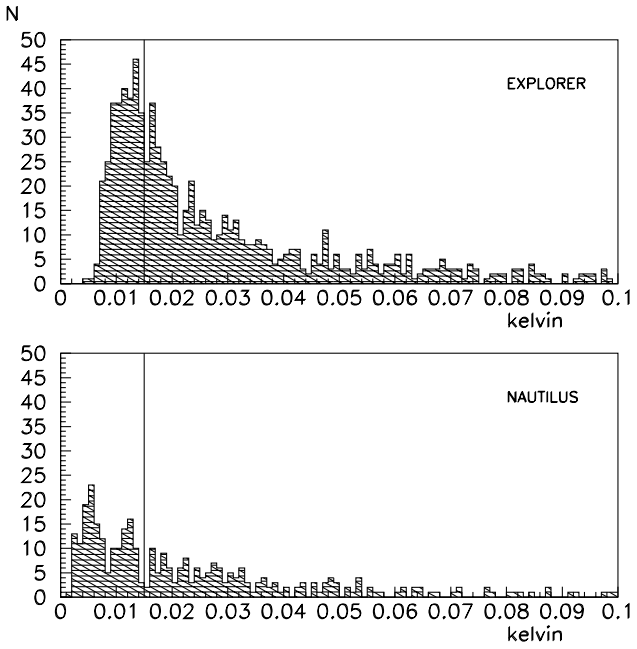

FIG. 1. Histograms of the effective temperature of the minimum mode of the Wiener filtered data computed in the 1150 time intervals of 30 min around each GRB time.

position of each source, which is an important parameter, because the sensitivity of a cylindrical bar GW detector is strongly dependent on the angle θ between the propagation direction of the wave and the axis of the cylinder.

The histogram of Fig. 2 shows the distribution of $\sin^4\theta$ for the 387 GRBs corresponding to the selected data stretches with $T_{\rm eff} \leq 15$ mK. The distribution has been compared to the theoretical distribution expected for isotropic sources by the Kolmogorov test [31]. The result of the test indicates a compatibility more than 0.9 in terms of probability. It means that in the present analysis there is no privileged direction. As we can note, the data sample is large enough to look for a statistical correlation between the presence of a GW energy excess at zero-delay and the value of $\sin^4\theta$. For this, the data set is divided into four equally populated ranges of $\sin^4\theta$, as indicated in Fig. 2 by the vertical lines, then these regions will be separately analyzed.

In the present work we use two algorithms, both based on coherent averages performed over the selected GW data stretches synchronized using the GRB flux peak time as a common reference in order to show a possible energy excess at zero-delay time within an integration time of 10 s [32].

The first algorithm computes the average of the data stretches corresponding to each GRB: we construct a new data stretch where at each time there is the average of the values, at that same time, of all the measured data stretches. The averaged energy at zero-delay is the measured physical quantity to be compared with the distribution of the

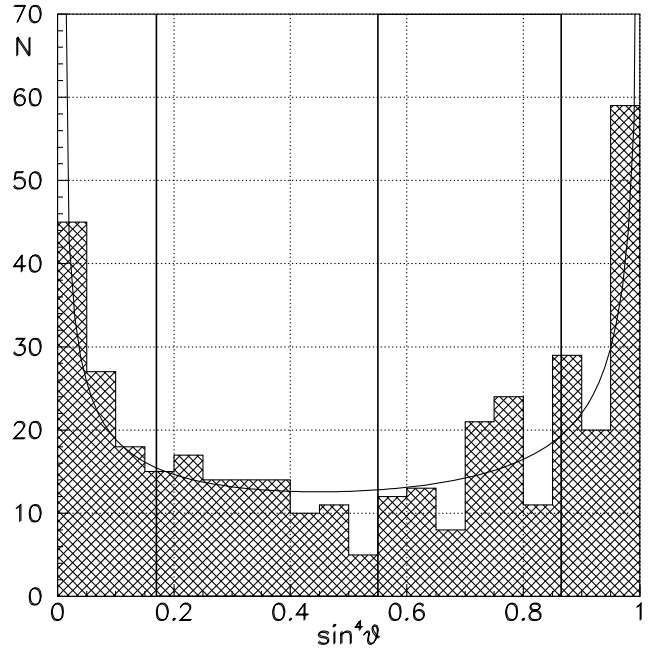

FIG. 2. Experimental histogram of $\sin^4\theta$ for the 387 GRB in the selected time intervals of 30 min around each GRB time (net area). The distribution is compared to theoretical isotropic distribution (solid line). The four regions of increasing $\sin^4\theta$, separated by vertical lines, correspond to the data subsets separately analyzed to look for a correlation with $\sin^4\theta$.

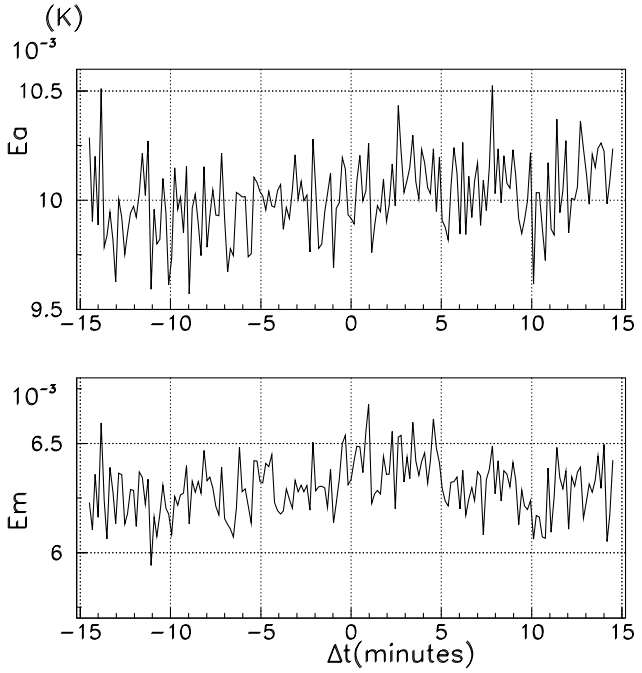

FIG. 3. Cumulative average (E_a) and cumulative median (E_m) of the GW detector energy as a function of the GW-GRB delay.

same averages taken at all the other times, constituting the background.

The second algorithm, which is a new one for this kind of analysis, differs from the first one since it uses the median of the data instead of the average. This is a robust way to detect the effect of many small synchronized contributions rather than that of a single or of a few very large signals. Indeed, it is easy to understand that a few intense spikes increase the variance of the average much more than that of the median. This is important also because the noise distribution of GW detectors data is affected by significant nongaussian tails, thus the occurrence of intense spurious noise spikes is not as unfrequent as it would be for an ideal detector with gaussian noise.

III. RESULTS AND DISCUSSION

In this work cumulative algorithms were used, searching for an energy excess above the background of the GW data at the GRB arrival time. Thus the results of this analysis, in terms of signal detected or upper limits, represent the average GW flux associated to each GRB and released simultaneously to the gamma emission, within a given time interval, telling nothing about the possibility of a much earlier and time-scattered GW emission. The analysis of a much larger time interval (30 min around the GRB time), which is performed in this work, has the purpose of estimating the background statistical distribution of the physical quantity that, computed at zero-delay, is assumed to be the indicator of correlation with GRBs.

In Fig. 3 the result of the application of the average algorithm is shown. The averaged GW detector energy innovation is plotted as a function of time, relative to the GRB flux peak time. In the same figure, the result of the application of the second algorithm is also reported. In this case, for each 10 s interval, the median of the distribution of the GW detector energy innovation measured in that interval is shown, as a function of the GW-GRB delay.

From the average and median time series shown in Fig. 3, $E_a(t)$ and $E_m(t)$, we consider the average and median value at zero-delay, $E_a(0)$ and $E_m(0)$, and compute the time averages $<E_a>$ and $<E_m>$, and the standard deviations σ_a and σ_m of the values at all other times, finding:

$$\text{average:}\quad E_a(0) = 9.91\,\text{mK},\quad <E_a> = 10.01\,\text{mK},\quad \sigma_a = 0.17\,\text{mK};$$
$$\text{median:}\quad E_m(0) = 6.33\,\text{mK},\quad <E_m> = 6.30\,\text{mK},\quad \sigma_m = 0.13\,\text{mK}.$$

The distributions show a good fit with the gaussian curves. For example, the agreement is shown in Fig. 4 for the distributions relative to the Fig. 3.

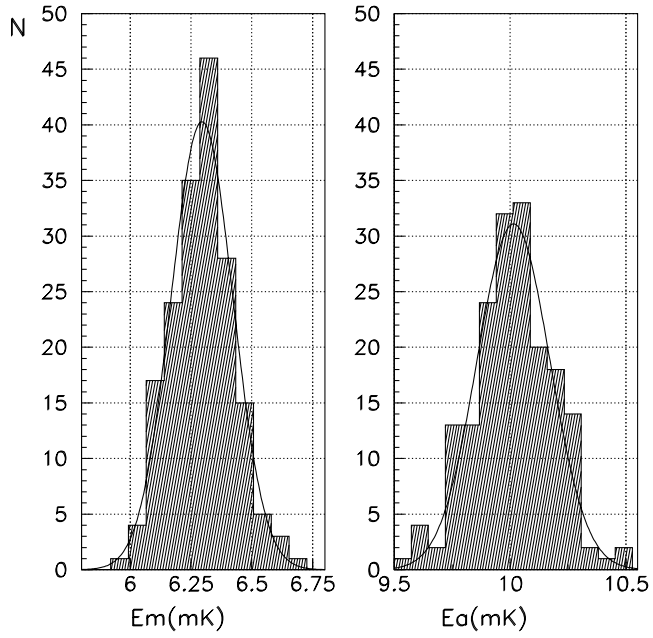

FIG. 4. Distributions of the median and of the average of the GW detector energy value (see Fig. 3) and gaussian fits.

With respect to the dependence of the observed energy value on $\sin^4\theta$, at zero-delay, the source direction information was used by separately analyzing the GRBs whose average $\sin^4\theta$ factor is within a given interval during the 30 min interval. The result of this analysis, shown in Fig. 5, was obtained applying the median algorithm to four subsets of GRBs, whose possible GW sources would be increasingly well-placed in the sky relative to the antenna axis, as expressed by their average value of $\sin^4\theta$. The quantity plotted in Fig. 5 is, for each subset, the signal-to-noise ratio, defined as:

$$\mathrm{SNR} \equiv \frac{E_m(0) - <E_m>}{\sigma}, \tag{3.2}$$

where $E_m(0)$ is the value of the median at zero-delay, $<E_m>$ and σ are the average and standard deviation of all the values at non-zero-delay in the cumulative median time series (see Fig. 3). The vertical bars indicate the uncertainty in SNR as deduced from the ones in $<E_m>$ and σ. No clear correlation (i.e., with SNR > 1) is visible in the data with the average value of $\sin^4\theta$.

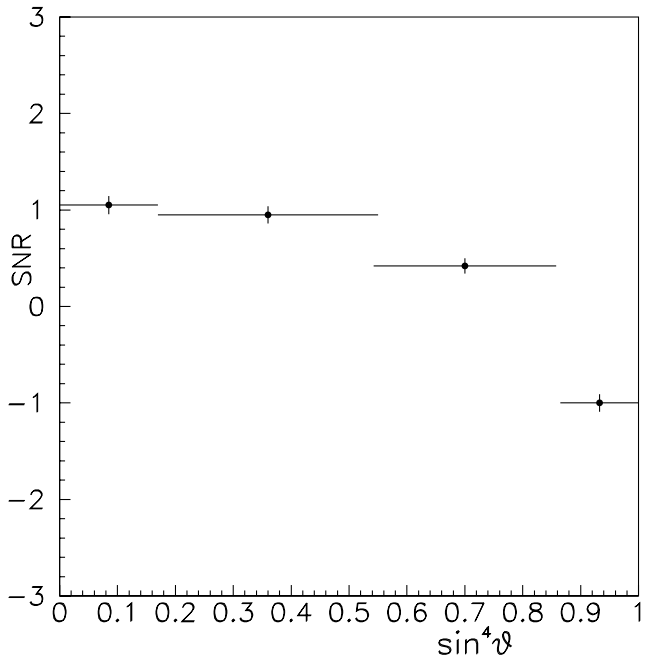

FIG. 5. SNR of the excess at zero-delay of the GW-median, as a function of $\sin^4\theta$.

IV. UPPER LIMIT EVALUATION

Figure 4 shows that both the average and median distributions are close to normal. This allows us to represent the sensitivity of the experiment as a function of h and to evaluate an upper limit, using the same approach followed in our previous GRB-GW coincidence analysis [13], based on the likelihood rescaled to its value for background alone (R function, called also *relative belief update function* [33]). In fact, in the Bayesian approach we are implicitly following, the likelihood has the role of modifying our knowledge according to the scheme *posterior* $\propto R\times$ *prior*. In presence of a signal with energy E_s we expect to measure an energy E_b larger by some quantity δ with respect to the case of no signal, that is:

$$E_b = E_n + \delta, \tag{4.1}$$

where E_n is due to noise. We indicate the measurement at zero time delay with E_0. Thus the expected normal distribution is

$$f(E_0|\delta) \sim e^{-[E_0-(E_n+\delta)]^2/2\sigma^2}, \tag{4.2}$$

where σ is the experimental standard deviation. We find the *relative belief updating ratio* R

$$R(\delta) = \frac{f(E_0|\delta)}{f(E_0|\delta=0)} = e^{-(\delta^2-2E_0\delta+2E_n\delta)/2\sigma^2}. \tag{4.3}$$

Using the quantities defined in the previous section, we can compute the functions $R_a(\delta_a)$ and $R_m(\delta_m)$, in the case of the average and median algorithm, respectively, and so we obtain an *upper limit*, or, better, an *upper sensitivity bound* on the value of δ_a and δ_m. If we take conventionally $R(\delta) = 0.05$, we determine

$$\delta_a(5\%) \sim 0.33 \text{ mK}, \qquad \delta_{\mathrm{m}}(5\%) \sim 0.35 \text{ mK}. \tag{4.4}$$

In order to find the relation between the increase δ_a and the corresponding value E_s of the signals that would generate it, we have to take into account that, as we discussed in Sec. II, we take time averages of 10 s, and this leads to a loss in sensitivity, since the signal due to a GW burst would

usually be shorter than 10 s. We evaluate this sensitivity loss in a factor 3.

In the case of the median algorithm, a further factor comes out: in the hypothesis of E_s much smaller that E_n, the distribution of $E_n + E_s$ remains exponential (as it was for E_n) and so if the average energy increases by E_s the median value increases by $E_s \ln 2$.

The energies $E_s^{a,m}$ corresponding to the values $\delta_{a,m}(5\%)$ are then

$$E_s^a \sim 1 \text{ mK}, \qquad E_s^m \sim 1.5 \text{ mK}. \tag{4.5}$$

The signal energy E_s is determined by the value of the Fourier transform $H(f)$ of the GW in the detector frequency band; computation of the GW burst amplitude h requires a model for the signal shape. A conventionally chosen shape is a featureless pulse lasting a time τ_g and giving a constant Fourier spectrum over a frequency band equal to $1/\tau_g$. Assuming the detector band within this range, for optimal orientation one has:

$$h = \frac{H}{\tau_g} = \frac{1}{\tau_g}\frac{L}{\upsilon_s^2}\sqrt{\frac{kE_s}{M}}, \tag{4.6}$$

where $\upsilon_s = 5.4$ km s^{-1} is the sound velocity in aluminum, L and M are the length and the mass of the bar, respectively. We conventionally assume a GW burst duration $\tau_g = 1$ ms, so the E_s values of Eq. (4.5) correspond to two quite close values for the sensitivity bound in h:

$$h_a \sim 2.5 \times 10^{-19}, \qquad h_m \sim 3.1 \times 10^{-19}. \tag{4.7}$$

The behavior of the *relative belief updating ratio* R as a function of h is given in Fig. 6, in both the average and median cases. We notice that in both cases, $R \simeq 1$ in the region with $h \leq 2 \times 10^{-20}$: this means that the detectors were not sensitive enough to appreciate such small amplitudes, and hence nothing can be learned from the experiment in that region of h.

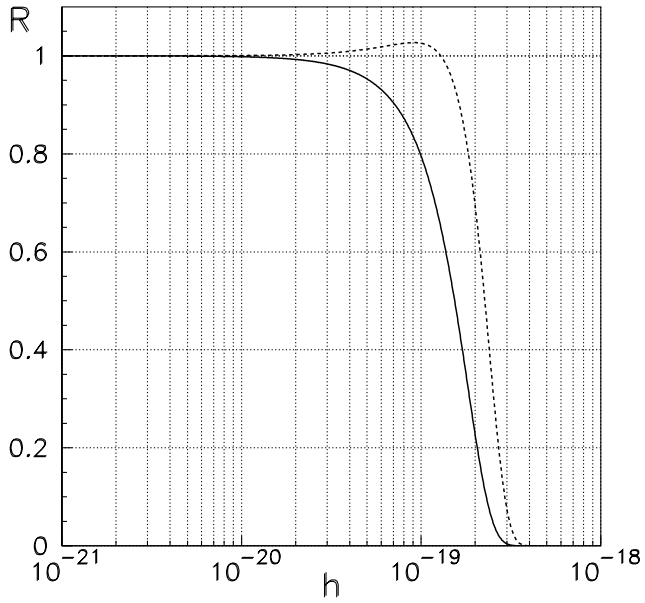

FIG. 6. *Relative belief updating ratio* as a function of h, using the average (solid line) and median (dashed line) algorithms.

V. CONCLUSIONS

A large sample of GRBs (387) was used to search for an association between the GW detector data and GRBs at zero-delay. No statistically significant excess was observed at zero-delay, within the time resolution of 10 s. We performed an analysis based on a Bayesian approach, obtaining an upper bound on the GW burst amplitude associated with GRB of $h \sim 2.5 \times 10^{-19}$.

ACKNOWLEDGMENTS

We thank Peter Saulson and other members of LSC for useful discussions and comments.

[1] G. J. Fishman and C. A. Meegan, Annu. Rev. Astron. Astrophys. **33**, 415 (1995).
[2] M. S. Briggs *et al.*, Astrophys. J. **459**, 40 (1996).
[3] G. Boella *et al.*, Astron. Astrophys. Suppl. Ser. **122**, 299 (1997).
[4] E. Costa *et al.*, Nature (London) **387**, 783 (1997).
[5] W. S. Paciesas *et al.*, Astrophys. J. Suppl. Ser. **122**, 465 (1999).
[6] C. Guidorzi *et al.*, in *Gamma-Ray Bursts in the Afterglow Era*, edited by E. Costa, F. Frontera, and J. Hjorth (Springer-Verlag, Berlin, 2001), p. 43.
[7] http://gammaray.msfc.nasa.gov/batse/grb/catalog/
[8] L. S. Finn, S. D. Mohanty, and J. D. Romano, Phys. Rev. D **60**, 121101 (1999).
[9] G. Modestino and G. Pizzella, Astron. Astrophys. **364**, 419 (2000).
[10] M. T. Murphy, J. K. Webb, and I. S. Heng, Mon. Not. R. Astron. Soc. **316**, 657 (2000).
[11] P. Bonifazi *et al.*, Astronomical and Astrophysical Transactions **22**, 557 (2003).
[12] G. Modestino and A. Moleti, Phys. Rev. D **65**, 022005 (2002).
[13] P. Astone *et al.*, Phys. Rev. D **66**, 102002 (2002).
[14] M. J. Rees and P. Mészáros, Astrophys. J., Lett. Ed. **430**, L93 (1994).
[15] T. Piran, Phys. Rep. **314**, 575 (1999).
[16] P. Mészáros, Science **291**, 79 (2001).
[17] B. Zhang and P. Mészáros, Int. J. Mod. Phys. A **19**, 2385 (2004).

[18] A. De Rujúla, astro-ph/0207033.
[19] S. Kobayashi and P. Mészáros, Astrophys. J. **589**, 861 (2003).
[20] M. H. P. M. van Putten, Phys. Rep. **345**, 1 (2001); M. H. P. M. van Putten *et al.*, Phys. Rev. D **69**, 044007 (2004).
[21] F. Frontera *et al.*, Astrophys. J. Suppl. Ser. **127**, 59 (2000).
[22] F. Frontera, *Lecture Notes in Physics*, (Springer, Berlin, Heidelberg, 2003), edited by K. W. Weiler vol. 598, p. 317.
[23] R. Sari, T. Piran, and R. Narayan, Astrophys. J., Lett. Ed. **497**, L17 (1998).
[24] G. Modestino *et al.*, in *Proceedings of Gravitational Wave Data Analysis Workshop 2, Orsay, 1997*, edited by M. Davier and P. Hello, p. 187.
[25] G. Modestino *et al.*, in *Proceedings of Frontier Objects in Astrophysics and Particle Physics, Vulcano, 1998*, edited by F. Giovannelli and G. Mannocchi, p. 295.
[26] P. Tricarico *et al.*, Phys. Rev. D **63**, 082002 (2001).
[27] P. Astone *et al.*, Classical Quantum Gravity **19**, 5449 (2002).
[28] S. D. Márka, talk given at *Gravitational Wave Data Analysis Workshop 8, Milwaukee, Wisconsin, 2003* (unpublished).
[29] A preliminary analysis of these data was presented at the 2003 Amaldi conference: P. Astone *et al.*, Classical Quantum Gravity **21**, S759 (2004).
[30] P. Astone, P. Bonifazi, G. V. Pallottino, and G. Pizzella, Nuovo Cimento Soc. Ital. Fis. C **17**, 713 (1994).
[31] W. T. Eadie, D. Drijard, F. L. James, and B. Saudoulet, *Statistical Method in Experimental Physics* (North-Holland Publishing Company, Amsterdam, 1971).
[32] The choice of 10 s as integration interval comes from estimating the possible differences between the *true* GRB arrival time and the flux peak time, and from the time resolution of our data. In principle, the optimal choice is to have an integration interval of the same order of the overall time uncertainty. This choice will imply losing sensitivity when the GW detector decay time is smaller than 10 s, which occurs about 50% of the times.
[33] G. D'Agostini, *Bayesian Reasoning in Data analysis* (World Scientific, Singapore, 2003).